ELSEVIER

Chemical Engineering Journal 140 (2008) 221–234

Chemical Engineering Journal

www.elsevier.com/locate/cej

Measurements and modeling of heat generation in a trickling biofilter for biodegradation of a low concentration volatile organic compound (VOC)

Qiang Liao [a,*], Xin Tian [a], Xun Zhu [a], Rong Chen [a], Yong Zhong Wang [a,b]

[a] *Institute of Engineering Thermophysics, Chongqing University, Chongqing 400044, PR China*
[b] *Academy of Bioengineering, Chongqing University, Chongqing 400044, PR China*

Received 16 March 2007; received in revised form 3 August 2007; accepted 26 September 2007

Abstract

The experimental and theoretical heat generation behavior of a trickling biofilter treating toluene is discussed. The experimental results show that the temperature of the packed bed has a significant effect on the purification performance of the trickling biofilter and that an optimal operation temperature exists between 30 and 40 °C. During the gas–liquid co-current flow, the temperature in the packed bed gradually rises along the direction of the gas and liquid flow due to the exothermic biodegradation of toluene. The temperature rise between the inlet and outlet of the trickling biofilter increases with an increase in the gas flow rate and inlet toluene concentration. In addition, a larger liquid flow rate leads to a smaller temperature rise. The heat generation process occurring in the trickling biofilter is modeled by representing the packed bed as an equivalent set of parallel capillary tubes covered by the biofilm. The temperature profile in the packed bed during the liquid–gas co-current flow is analyzed by simultaneously solving the problem of gas–liquid two-phase flow and heat and mass transfer through the liquid film and biofilm. It is shown that the model agrees well with the experimental data, predicting the variations of the temperature rise between the inlet and outlet of trickling biofilter with the increasing gas and liquid flow rates.

Keywords: Trickling biofilter; Gas–liquid co-current flow; Capillary tube model; Temperature profile; Toluene

1. Introduction

In recent years, with increasingly stringent regulations of air emissions of volatile organic compounds (VOCs), an economical control technology has been needed [1]. Biofiltration offers a number of economical and environmental advantages over conventional technologies such as incineration, catalytic oxidation, adsorption, and chemical scrubbing. It has become one of the leading technologies for controlling VOC emissions [2,3]. There are three conventional types of biofilter: biofilter, trickling biofilter, and bioscrubber. Trickling biofilters have been shown in several instances to be superior to biofilters when accurate control of the environmental conditions or higher pollutant elimination rates is required [4]. Moreover, trickling biofilters packed with materials with better structural strength can be built taller than biofilters [5]. A trickling biofilter consists of a porous packed bed of inorganic or synthetic material, on the surface of which biofilm is developed during the process of start-up. A liquid stream trickles through the porous packed bed and provides non-carbon-containing nutrients to the microorganism. The microorganism in the biofilm degrades the biodegradable pollutants in waste gas while it passes through the packed bed and diffuses through the attached biofilm.

In recent years, considerable experimental studies on the purification performance of trickling biofilters have been conducted for the treatment of VOCs [6–8]. Some representative mathematical models were established to simulate the biodegradation of VOCs in a trickling biofilter [9–11]. The capability of microorganisms to degrade pollutants is closely related to environment conditions. Temperature is an important consideration. Because temperature has a direct influence on the degradation performance of microorganisms, it is the key concern in all biological treatment systems. Temperature control is a vital factor for efficient biofilter operation, and in many practical applications temperature controls are added to the biofilter systems to prevent thermal shocks [12,13]. Bed temperatures are also

* Corresponding author. Tel.: +86 23 65102474; fax: +86 23 65102474.
E-mail address: lqzx@cqu.edu.cn (Q. Liao).

1385-8947/$ – see front matter © 2007 Elsevier B.V. All rights reserved.
doi:10.1016/j.cej.2007.09.043

Nomenclature

a	specific surface area of packed material (m^{-1})
a_l	specific active biofilm surface area of trickling biofilter (m^{-1})
A_T	cross-sectional area of the trickling biofilter column (m^2)
c_p	thermal capacity ($J\,kg^{-1}\,K^{-1}$)
C_{bO}	concentration of oxygen in biofilm ($g\,m^{-3}$)
C_{bT}	concentration of pollutant in biofilm ($g\,m^{-3}$)
C_{gO}	concentration of oxygen in gas phase ($g\,m^{-3}$)
C_{gT}	concentration of pollutant in gas phase ($g\,m^{-3}$)
C_{lO}	concentration of oxygen in liquid film ($g\,m^{-3}$)
C_{lT}	concentration of pollutant in liquid film ($g\,m^{-3}$)
D_{bO}	diffusion coefficient of oxygen in biofilm ($m^2\,s^{-1}$)
D_{bT}	diffusion coefficient of pollutant in biofilm ($m^2\,s^{-1}$)
D_{lO}	diffusion coefficient of oxygen in liquid film ($m^2\,s^{-1}$)
D_{lT}	diffusion coefficient of pollutant in liquid film ($m^2\,s^{-1}$)
D_p	diameter of ceramic spheres (m)
D_T	diameter of trickling biofilter (m)
g	acceleration of gravity ($m\,s^{-2}$)
h	height of packed bed (m)
K_{IT}	self-inhibition kinetic constant for biodegradation of pollutant ($g\,m^{-3}$)
K_O	kinetic constant for biodegradation of oxygen ($g\,m^{-3}$)
K_T	kinetic constant for biodegradation of pollutant ($g\,m^{-3}$)
m	Henry's constant
M_T	molecular weight of toluene
n_c	number of capillary tubes
p	static pressure of gas and liquid in capillary tube (Pa)
p_c	capillary pressure (Pa)
Pe	Peclet number
q	volume flow rates in capillary tube ($m^3\,s^{-1}$)
Q	volume flow rates in trickling biofilter ($m^3\,h^{-1}$)
r_b	radius at the interface of biofilm and liquid film in capillary tube (m)
r_l	radius at the interface of gas–liquid in capillary tube (m)
r_s	radius of capillary tube (m)
T_b	temperature in the biofilm (°C)
T_{gl}	temperature in the gas core and liquid film (°C)
u	velocity in capillary tube ($m\,s^{-1}$)
x	x-axis in the packed bed of trickling biofilter (m)
X_V	dry density of biofilm ($kg\,m^{-3}$)
Y_T	yield coefficient of a culture on pollutant

Greek symbol

β_b	dimensionless number, $\beta_b = \frac{\Delta H_R^s X_V \mu_{max} r_s^2}{\lambda_b T_{in} Y_T}$
β_{gl}	dimensionless number, $\beta_{gl} = \frac{2h\lambda_b r_b}{[\rho_g c_{p,g} \mu_g r_l^2 + \rho_l c_{p,l} u_l (r_b^2 - r_l^2)] r_s}$
β_i	dimensionless number, $\beta_i = X_V \mu_{max} r_s^2/(Y_T D_{bi} C_{gi,in})$, i = T,O
δ_e	thickness of the active biofilm (μm)
ε	porosity of packed bed in trickling biofilter
η	purification efficiency of trickling biofilter
λ	thermal conductivity ($W\,m^{-1}\,K^{-1}$)
μ	dynamic viscosity ($N\,S\,m^{-2}$)
μ_{max}	maximum specific growth rate of microorganism (h^{-1})
ρ	density ($kg\,m^{-3}$)
σ_l	liquid surface tension ($N\,m^{-1}$)
σ_p	surface tension of packing material ($N\,m^{-1}$)
ξ	correction factor

Superscripts

*	dimensionless number

Subscripts

b	biofilm
g	gas phase
in	inlet of trickling biofilter
l	liquid film

an indicator of the intensity of microbial activity [14]. There are three general temperature classes of aerobic microorganisms: psychrophilic microorganisms that grow best below a temperature of 20 °C; mesophilic microorganisms that achieve highest growth rates between 20 and 40 °C, and thermophilic microorganisms that grow best at temperatures above 45 °C [12]. The biological reactions stop if the temperature is not suitable for the growth of the microorganisms. Cox et al. [5] reported the experimental results of the temperature shock effect on the performance of a trickling biofilter treating ethanol. The experimental results indicated that the performance of the ambient-temperature reactor without thermophilic microorganisms apparently decreased with increasing temperature, and the upper temperature limit of the high-temperature reactor hosting a process culture composed of both mesophilic and thermotolerant or thermophilic microorganisms was 62 °C. Lu et al. [15] found experimentally that the removal efficiency of a trickling biofilter treating benzene, toluene, ethylbenzene and *o*-xylene (BTEX) vapors increased with an increase in the operating temperature in the range of 15–30 °C. However, an opposite trend was observed between 30 and 50 °C.

In general, the metabolic biodegradation of the organic pollutants is an exothermic process. Therefore, the temperature of the biofilter bed increases gradually in the gas flow direction [16]. Furthermore, the temperature of the packed bed increases with an increase in the metabolizing intensity of microorganisms. Jorio et al. [17] found experimentally that

the temperature increased from 23 to 28 °C during the first 20 days following the start-up of the biofilter at a gas flow rate of 1 $m^3 h^{-1}$. Nikiema et al. [18] examined the biofilter bed temperature increase between the inlet and outlet ports of two biofilters, one composed of inorganic material and the other of mature compost. The experimental results revealed that the temperature difference was less than 1 °C over all stages of the biofilter packed with inorganic material, whereas in the mature compost biofilter, the temperature difference was significantly greater, up to 2.8 °C, when the nitrogen concentration was greater than 0.5 g N L^{-1}. Kiared et al. [16] monitored temperature in the biofilter bed for diagnosing the intensity of microbial metabolism. It is shown by the experimental results that a major increase in the toluene elimination capacity from 25 to 160 g h^{-1} m^{-3} led to a bed temperature rise from 25 to 38 °C. William and Miller [19] studied the effect of temperature on the microorganism activity and found that biological activity roughly doubles for each 10 °C rise in temperature of the biofilter bed, to an optimum temperature of about 37 °C for mesophilic bacteria. Marsh [20] found that an inlet gas temperature exceeding 40 °C had a great effect on the biofilter performance, and cooling of the gas stream is necessary. This can be achieved through dilution with ambient air or in a pre-humidification chamber. Similarly for cold air streams below 10 °C heating of the gas stream to a desirable temperature is needed, as microorganisms are relatively inactive at low-temperatures. Rozich [13] reported that large changes in temperature disrupt the biological system and decrease overall system performance.

As described above, the temperature of a packed bed has a significant effect on the biodegradation activity of microorganisms. Simultaneously, the temperature profile depends on the exothermic reaction and heat transfer in the packed bed. Therefore, the heat transfer characteristic in the porous packed bed needs to be studied to understand the interaction between the heat generation and treatment performance. To the best of our knowledge, the majority of previous work concentrated on studying the purification behavior of trickling biofilters and the effect of temperature on the purification performance. A few studies [21–23] worked on the mass transfer model to obtain the biodegradation performance. However, these models are not enough to predict the characteristics of heat transfer coupled with mass transfer and the biochemical reaction kinetics as a function of the temperature. In this work, a combined experimental and theoretical study was carried out to investigate the heat generation and transfer in a trickling biofilter for the VOC waste gas removal. First, the purification efficiencies and temperature profiles of a trickling biofilter were measured for variations in the gas flow rate, liquid flow rate, and inlet toluene concentration. Based on the experimental investigations, the heat generation and heat transfer processes in the trickling biofilter were then modeled.

In the following, our experimental work will be discussed first. A theoretical analysis of the problem based on heat and mass transfer in the liquid film and the biofilm of a capillary tube will then be presented. Finally, the important findings of the study will be summarized.

2. Experimental study

2.1. Experimental set-up

A representation of the experimental system used in the present investigation is shown in Fig. 1. This consisted of three major parts: the liquid supply system, the gas supply system, and the trickling biofilter. The liquid supply system consisted of a circulation liquid container with a nutrient supply, two circulation pumps, an electric heater, and a tube-shell heat exchanger. The liquid pumped from the circulation liquid container was bifurcated into two streams: one stream was delivered through the tube-shell heat exchanger into a liquid distributor at the top of the trickling biofilter and then trickled down under gravity as the nutrient feed while the remainder returned through a electric heater to the circulation liquid container for the adjustment of the circulation liquid flow rate. The tube-shell heat exchanger with a constant temperature bath that had a range from room temperature to −20 °C and the electric heater were installed to keep the circulation liquid temperature to a desired value between 0 and 70 °C. The temperature of the packed bed in the trickling biofilter was controlled by adjusting the circulation liquid temperature with the tube-shell heat exchanger and the electric heater. The gas supply system consisted of a compressed air jet, a pressure stabilizer, a pure toluene bottle, and a mixing chamber. The airflow expelled from the compressed air jet passed through a pressure stabilizer into the bottle of pure toluene, in which the bubbly airflow enhanced the evaporation of liquid toluene. The toluene vapor and carried gas entered the trickling biofliter at the top (the gas–liquid co-current flow mode), or at the bottom (the gas–liquid counter-current flow mode). The room temperature was regulated by an air conditioner.

The vertically oriented trickling biofilter was made from stainless steel cylinder with a 0.3 m internal diameter, 3 mm thickness, and 1.4 m height. It was packed with ceramic spheres 0.018 m in diameter and the height of the packed bed was 0.5 m. At the top of the trickling biofilter, a liquid distributor was installed to keep a uniform liquid distribution in the packed bed. A perforated plate was installed at the bottom of the trickling biofilter to hold the ceramic spheres in place during the experiments. The biofilter body was wrapped with polyurethane foam 0.02 m in thickness for thermal insulation.

Before start-up, the biofilter was seeded with a consortium of microbial species originated from an activated sludge system utilizing hydroxybenzene as one of the carbon sources. The sample was first exposed to toluene in a batch culture before being inoculated in the recirculation liquid container and then the original pure-culture strain of the toluene-degrading bacterium, *Pseudomonas putida*, was isolated. Finally, the inoculation was made under non-sterile conditions in the circulation liquid container, and the biofilm grew gradually on the surface of the packed materials with the supplying of the toluene exhaust gas and the liquid replenished with fresh growth medium solution through the trickling biofilter. The nutrient solution was composed of inorganic salts with a nitrogen-to-phosphorous ratio of 5:1 including 21.75 g $K_2HPO_4 \cdot H_2O$, 33.48 g $Na_2HPO_4 \cdot 12H_2O$, 5 g NH_4Cl, 8.5 g KH_2PO_4, 22.5 g

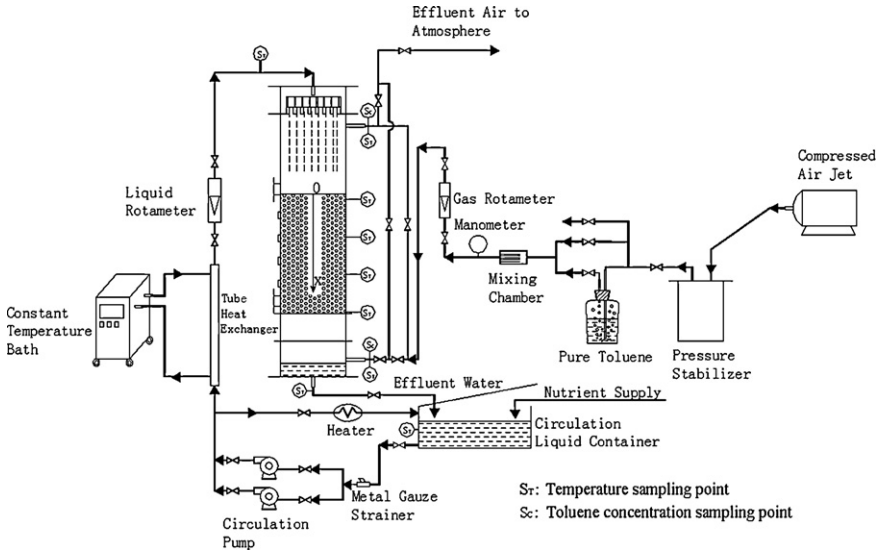

Fig. 1. Schematic of the experimental set-up.

$MgSO_4$, 36.4 g $CaCl_2$, 0.25 g $FeCl_3$, 0.04 g $MnSO_4{\cdot}H_2O$, 0.04 g $InSO_4{\cdot}H_2O$, and 0.03 g $(NH_4)_6Mo_7O_{24}{\cdot}4H_2O$ per liter of distilled water, to grow microorganisms in an environment of carbon and essential nutrients. pH 7.0 ± 0.1 was maintained using Na_2HPO_4 and NaH_2PO_4.

2.2. Analytical methods

The temperature profile of the packed bed was measured with 12 T-type thermocouples 0.2 mm in diameter. The locations of the thermocouples are shown in Fig. 2. Thermocouples were inserted in the packed bed at distances of 0.02, 0.18, 0.34, and 0.5 m from the bed top (see Fig. 2). The bed temperature was obtained by averaging the readings of the three thermocouples at each level. Four T-type thermocouples 0.2 mm in diameter were used to measure the circulation liquid temperature at the liquid-line inlet and outlet. Two T-type thermocouples were installed at the gas-line inlet for measuring the inlet temperature of waste gas. A data acquisition system was employed to record the temperature measurements.

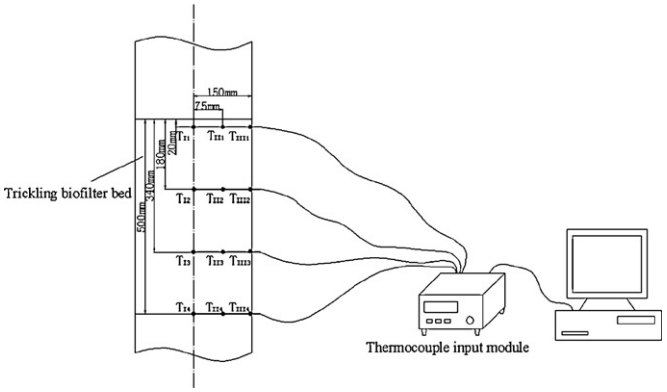

Fig. 2. Arrangement and locations of thermocouples in the trickling biofilter.

The gas-phase measurements included the flow rate and the concentration of toluene at the inlet and outlet of the trickling biofilter. The flow rate of waste gas was measured with a gas-type rotameter. The toluene concentration was measured using a gas chromatograph (GC) equipped with a flame ionization detector (FID) while the carrier gas (N_2) flow rate was set at 30 mL min^{-1} and the GC oven temperature and FID temperature were maintained at 80 and 170 °C, respectively. Liquid-phase samples were measured for flow rate, absorbency ($OD_{600\,nm}$) and pH. The measurement of $OD_{600\,nm}$ of the circulation liquid was carried out using a spectrophotometer and the pH value was measured by a pH meter calibrated with buffers (pH of 4.0 and 7.0) supplied by the manufacturer. The flow rate of the circulation liquid was measured with a liquid rotameter.

In order to stabilize the thermal status in the packed bed, prior to each experiment, the temperature of the circulation liquid was adjusted and kept constant for 24 h. In the present study, the circulation liquid flow rate (Q_l) ranged from 0.009 to 0.020 $m^3\,h^{-1}$ and the gas flow rate (Q_g) from 0.4 to 1.6 $m^3\,h^{-1}$ at room temperature (about 25–28 °C). The performance of the trickling biofilter was assessed with the elimination capacity (EC, g $m^{-3}\,h^{-1}$) and efficiency, which are defined as:

$$\mathrm{EC} = \frac{(C_{gT,in} - C_{gT,out}) \times Q_g}{V_b}, \tag{1}$$

$$\eta = \frac{C_{gT,in} - C_{gT,out}}{C_{gT,in}} \times 100\%, \tag{2}$$

where C_{gT} presents the concentration of the pollutant (g m^{-3}), and the subscripts 'in' and 'out' stand for the parameter at the inlet and outlet of the trickling biofilter. Q_g is the gas flow rate ($m^3\,h^{-1}$), and V_b is the volume of the packed bed (m^3).

2.3. Experimental results

2.3.1. Effect of temperature in the packed bed on the purification performance of the trickling biofilter

Experiments were conducted to investigate the effect of temperature in the packed bed on the purification performance of the trickling biofilter. During the experiments, the inlet toluene concentration was maintained at 1.2 g m^{-3}, the gas flow rate at 0.8 m^3 h^{-1}, and the liquid flow rate at 0.016 m^3 h^{-1}, respectively. The inlet toluene load of the trickling biofilter was 27.2 g m^{-3} h^{-1}. The temperature of the circulation liquid was regulated by the constant temperature bath and the electric heater to maintain the temperature of the packed bed at various required values. After the temperature of the packed bed was held constant for 24 h, the purification efficiency and the elimination capacity of the trickling biofilter were measured. The experimental results are shown in Fig. 3, where the triangular symbols and the square symbols represent the measured data of purification efficiency and elimination capacity, respectively. It is shown that with an increase in temperature in the packed bed, both the purification efficiency and the elimination capacity of the trickling biofilter gradually increased, reached a peak value, and dropped rapidly afterwards. Obviously, the temperature has a significant effect on the purification performance of the trickling biofilter. It can be seen from Fig. 3 that the purification efficiency and elimination capacity could be more than 90% and 12 g m^{-3} h^{-1} between packed bed temperatures of 30 and 40 °C, while these parameters were just 43% and 5.9 g m^{-3} h^{-1} at 60 °C. There exists an optimal operation temperature range for toluene removal using the trickling biofilter in the present experiment. It can be concluded that the purification performance of the trickling biofilter in treating toluene is sensitive to the temperature change of the packed bed. Furthermore, the temperature of the packed bed is significantly affected by the two-phase flow, heat and mass transfer, and heat generation during biodegradation. As such, it is necessary to quantify the temperature behavior in the packed bed of the trickling biofilter. For these reasons, experiments on the temperature behavior at various gas flow rates, liquid flow rates, and inlet toluene concentrations were conducted, and a theoretical model was established to predict the temperature behavior in the packed bed of a trickling biofilter.

2.3.2. Temperature profile along the axial direction of the trickling biofilter

The variation of the temperature in the packed bed along the axial direction of the trickling biofilter at four different horizontal locations are plotted in Fig. 4 for different liquid flow rates at the same gas flow rate (Q_g = 1.6 m^3 h^{-1}) and the same inlet toluene concentration ($C_{gT,in}$ = 2.5 g m^{-3}) in the co-current flow mode. The reason for this choice of inlet toluene concentration is to provide an excess inlet toluene load (113.2 g m^{-3} h^{-1}) for the biochemical reaction and to allow for the biochemical kinetics to be dominant. When the biochemical kinetics is dominant over the mass transfer of toluene, the change in temperature will significantly affect the performance of the trickling biofilter. It can be seen that the temperature of the packed bed gradually increased in the flow direction of gas and liquid for a fixed operation condition. The largest temperature rise was near 2.0 °C, implying that the biodegradation of toluene in the trickling biofilter was an exothermic process. The temperature rise of the packed bed decreased with an increase in the circulation liquid flow rate for a specific inlet toluene concentration and gas flow rate. This is due to the fact that a larger liquid flow rate leads to a thicker liquid film covering the biofilm on the solid medium, which caused an increase in the mass transfer resistance of toluene from the gas-phase region to the biofilm region. Therefore, the elimination capacity of toluene in the trickling biofilter decreased. The effect of liquid flow rate on the elimination capacity of the trickling biofilter has been found in previous experimental works [6,24–26]. In the present experiments, the measured purification efficiency and elimination capacity of the trickling biofilter were 65% and 74 g m^{-3} h^{-1} for a liquid flow rate of 0.009 m^3 h^{-1} while they reduced to 48% and 58 g m^{-3} h^{-1} for a liquid flow rate of 0.02 m^3 h^{-1} as shown

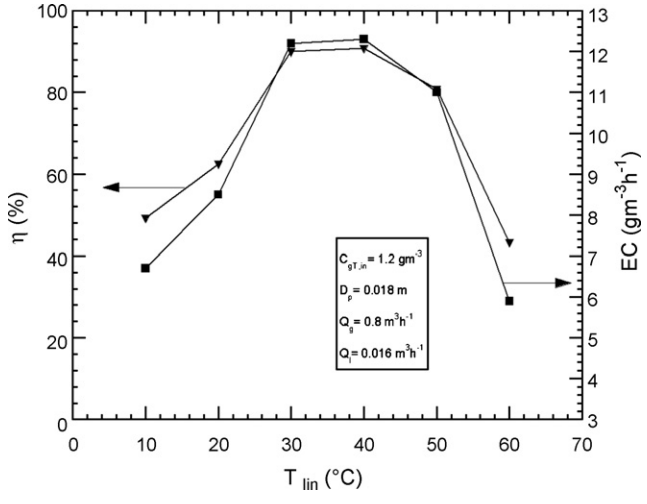

Fig. 3. Effects of the circulation liquid temperature on the purification performance of the trickling biofilter.

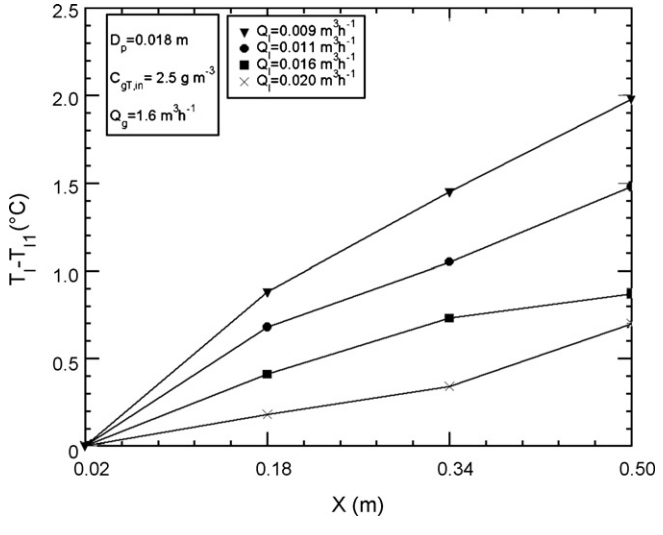

Fig. 4. Temperature profiles in the trickling biofilter at different liquid flow rates for Q_g = 1.6 m^3 h^{-1} and $C_{gT,in}$ = 2.5 g m^{-3}.

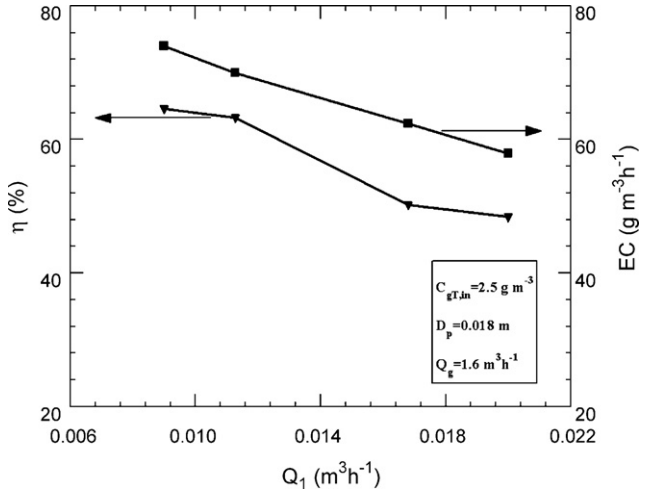

Fig. 5. Effects of the liquid flow rate on the purification performance of the trickling biofilter.

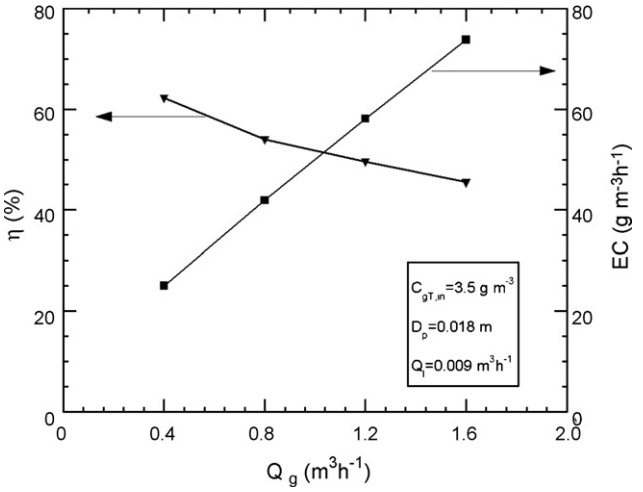

Fig. 7. Effects of the gas flow rate on the purification performance of the trickling biofilter.

in Fig. 5. This is the main reason why the heat generation of biodegradation reduced since it is proportional to the elimination capacity of the trickling biofilter. The increase in the circulation liquid flow rate resulted in a reduction in the temperature rise in the packed bed at a fixed heat generation of biodegradation from a viewpoint of energy balance. As such, it is concluded that the temperature rise of the packed bed increases as the circulation liquid flow rate decreases.

The effect of the gas flow rate on the temperature rise of the packed bed for $Q_l = 0.009\,m^3\,h^{-1}$ and $C_{gT,in} = 3.5\,g\,m^{-3}$ is presented in Fig. 6. It is noted that the temperature rise of the packed bed increased as the gas flow rate increased from 0.4 to 0.8, 1.2 and 1.6 $m^3\,h^{-1}$. The increase in the temperature rise can be explained by the variation of elimination capacity with the gas flow rate shown in Fig. 7. It is seen from this figure that for the same circulation liquid flow rate and the same inlet toluene concentration, the elimination capacity increased as the gas flow rate increased even though the purification efficiency decreased. This experimental result was consistent with previous studies [24,25]. At a fixed inlet toluene concentration, a larger gas flow rate represented a higher toluene loading, which increased the mass transfer of toluene from the gas-phase region to the biofilm region in the packed bed and caused an increase in the elimination capacity of toluene. A larger elimination capacity of toluene means a larger heat generation in the biodegradation of toluene, therefore, the temperature rise of the packed bed increases. It should be noted that the heat load required to maintain the temperature rise of the packed bed becomes larger with an increase of the gas flow rate, which has a negative effect on the temperature rise of the packed bed. However, because the waste gas has a smaller density and specific heat capacity, the effect should be insignificant compared to the increase in the heat generation of biodegradation.

Fig. 8 shows the temperature profiles in the packed bed at different inlet toluene concentrations for the same gas flow rate ($Q_g = 1.6\,m^3\,h^{-1}$) and circulation liquid flow rate

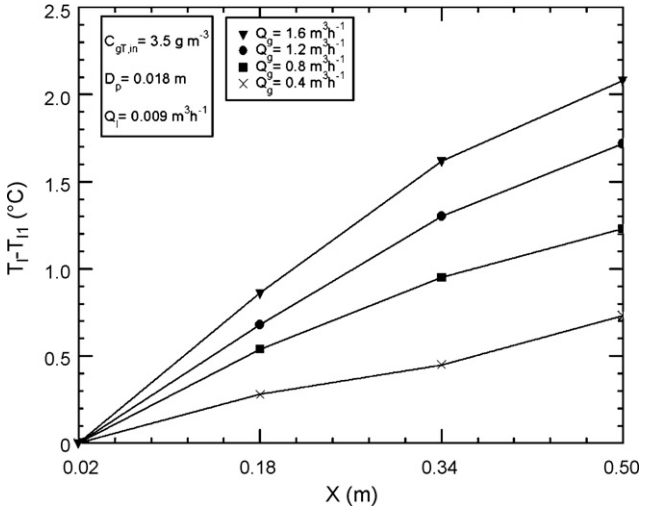

Fig. 6. Temperature profiles in the trickling biofilter at different gas flow rates for $Q_l = 0.009\,m^3\,h^{-1}$ and $C_{gT,in} = 3.5\,g\,m^{-3}$.

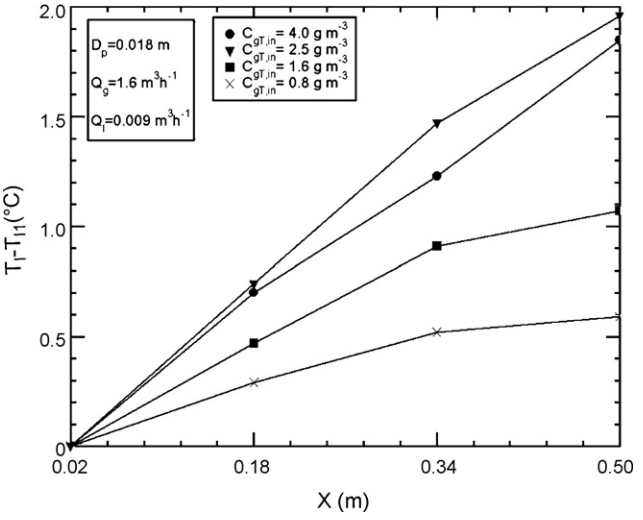

Fig. 8. Temperature profiles in the trickling biofilter at different inlet toluene concentrations for $Q_g = 1.6\,m^3\,h^{-1}$ and $Q_l = 0.009\,m^3\,h^{-1}$.

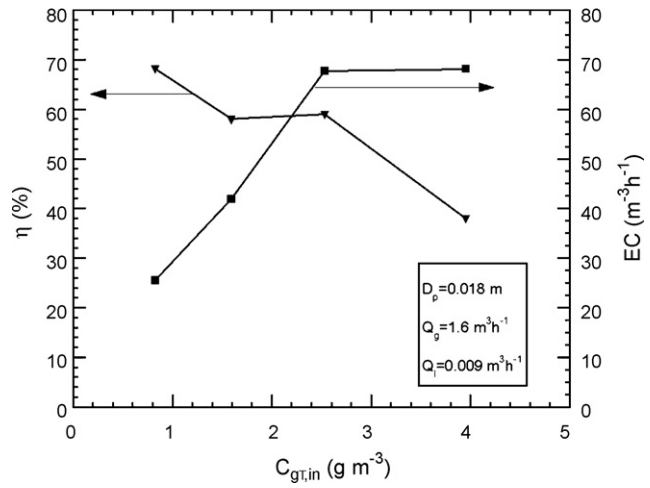

Fig. 9. Effects of the inlet toluene concentration on the purification performance of the trickling biofilters.

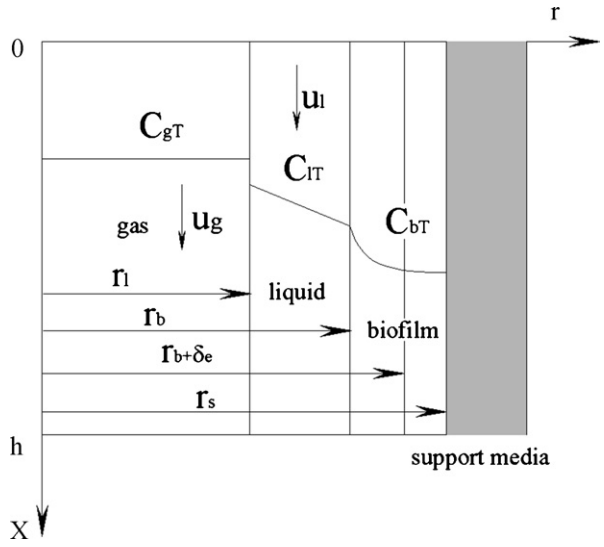

Fig. 10. Schematic of the physical model for the trickling biofilter with gas–liquid co-current flow.

($Q_l = 0.009\ m^3\ h^{-1}$). It is seen from this figure that the temperature difference in the packed bed increased with an increase in the inlet toluene concentration at a constant gas flow rate and circulation liquid flow rate. This is because the elimination capacity of the trickling biofilter is increased with the increase in the inlet toluene concentration, which is confirmed by the experimental results of purification performance as shown in Fig. 9. A larger elimination of toluene induced more heat generation. However, it should be noted from Fig. 8 that the effect of the inlet toluene concentration on the temperature rise of the packed bed became inconspicuous at a higher inlet toluene concentration. The primary reason was because the long-term exposure to a higher toluene concentration has a toxic effect on the biofilm and results in the inactivation of a major part of the biofilm [3,27–29]. Therefore, the increase in the elimination capacity of the trickling biofilter becomes slight as the inlet toluene concentration is further increased. Fig. 9 shows the elimination capacity of the trickling biofilter was 68.1 g m^{-3} h^{-1} at the inlet toluene concentration of 4.0 g m^{-3} and 67.7 g m^{-3} h^{-1} at the inlet concentration of 2.5 g m^{-3}. As such, the temperature rise of the packed bed increased a little as the inlet toluene concentration was raised from 2.5 to 4.0 g m^{-3}.

3. Theoretical study

Following the hydraulic radius model [30], which has been applied in the analysis of the flow behavior and boiling heat transfer behaviors in a porous medium [31,32], the porous packed bed of the trickling biofilter in the present study can be simulated as a series of straight capillary tubes covered by biofilm. Liquid flows downward and the waste gas is forced downward in the gas–liquid co-current flow mode. The schematic of the physical problem is shown in Fig. 10. There are three zones in the capillary tube: the biofilm over the tube wall ($r_b \le r \le r_s$), the thin liquid film over the biofilm ($r_l \le r \le r_b$), and the gas core in the center of the tube ($0 \le r \le r_l$). In the biofilm, there exist two zones: the reaction free zone ($r_b + \delta_e \le r \le r_s$) and the reaction zone ($r_b \le r \le r_b + \delta_e$) as indicated by Ottengraf and Oever [33]. The transport and biodegradation process of pollutant and oxygen in the physical domain can be recapitulated as the pollutant and oxygen in the waste gas that flows in the gas core being firstly absorbed at the liquid–gas interface, then diffused in the liquid film and biofilm, and finally degraded by microorganisms in the biofilm. The microorganisms in the biofilm metabolize the organic substances which are decomposed into water and carbon dioxide by the biochemical reaction accompanied with heat release.

The radius of the capillary tube can be expressed as [30]:

$$r_s = \frac{2\varepsilon}{a(1-\varepsilon)}, \tag{3}$$

where ε is the porosity of the packed bed and a is the specific surface area of the packed material (m^{-1}). During steady operation, the thickness of the biofilm was considered to be 0.1 times the radius of the packed material [34]. The thickness of the biofilm should be taken into account in determination of the porosity and specific surface area of the packed bed. As indicated in Fig. 10, the gas–liquid flow field through the tube is divided into the liquid film flow on the biofilm and the gas core flow in the center. In the present model, the velocity distribution in the gas core and the liquid film and the liquid film thickness in the capillary tube are obtained by solving a set of momentum conservation equations. The mass transport equations combined with biochemical kinetics equation are then established for the pollutant concentration profile in the gas core, the liquid film, and the biofilm, in which the effect of mass transport resistance in the liquid film and the biofilm, the gas–liquid interfacial mass transport resistance has been taken into account. Finally, the energy conversation equations in the gas core, the liquid film, and the biofilm are individually established to determine the temperature profile in the packed bed of the trickling biofilter using the pollutant concentration profile in the liquid film and the biofilm obtained by solving the formerly mentioned mass transport equations. The model assumptions are as follows: (1) the biofilm is formed on

the exterior surface of the packed materials, thus, no reaction occurs in the pores of the packed materials; (2) the thickness of the biofilm is uniform around the packed materials; (3) the size and distribution of particles in the trickling biofilter are uniform; (4) the gas flow and liquid flow are one-dimensional fully developed flow in the axial direction; (5) the diffusion of the VOC, oxygen, and the heat conduction are in the direction normal to the biofilm. Axial diffusion and heat conduction are neglected; (6) convective mass transport in the liquid film zone is neglected; (7) the absorption of VOC pollutant and oxygen at the gas–liquid interface can be evaluated with Henry's law; (8) there is no biomass in the gas core and the liquid film; (9) carbon dioxide and water are the final products of biodegradation; (10) the influence of temperature on the physical properties is ignored; (11) the surface of packed materials is adiabatic and (12) the VOC concentration difference, the oxygen concentration difference and the temperature difference in the gas core and the temperature difference in the liquid film along the radial direction are neglected due to a smaller pore size of the porous medium and a smaller biodegradation quantity and heat release.

3.1. Thickness of liquid film under the gas–liquid co-current flow

Consider the two-phase co-current flow of liquid and gas through the capillary tube as shown in Fig. 10. The governing conservation momentum equation in the gas core zone ($0 \le r \le r_l$) can be written as:

$$\mu_g \frac{1}{r}\frac{d}{dr}\left(r\frac{du_g}{dr}\right) - \frac{dp_g}{dx} = 0, \tag{4}$$

with corresponding boundary conditions for co-current flow,

$$\text{at } r = 0, \quad \frac{du_g}{dr} = 0, \tag{5}$$

$$\text{at } r = r_l, \quad u_g = u_l, \tag{6}$$

where μ is dynamic viscosity ($N\,s\,m^{-2}$); p the static pressure (Pa); u the velocity ($m\,s^{-1}$); the subscript 'g' and 'l' represent gas phase and liquid film in the capillary tube, respectively.

As the liquid flow rate is smaller, the liquid passes through the trickling biofilter in laminar flow. Thus, the conservation momentum equation in the liquid film zone is

$$\mu_l \frac{1}{r}\frac{d}{dr}\left(r\frac{du_l}{dr}\right) + \rho_l g - \frac{dp_l}{dx} = 0, \tag{7}$$

with corresponding boundary conditions for co-current flow,

$$\text{at } r = r_l, \quad \mu_l\frac{du_l}{dr} = \mu_g\frac{du_g}{dr}, \tag{8}$$

$$\text{at } r = r_b, \quad u_l = 0, \tag{9}$$

where ρ is the density ($kg\,m^{-3}$), and g is the acceleration of gravity ($m\,s^{-2}$).

Integrating Eqs. (4) and (7) subject to the boundary conditions (5), (6), (8) and (9) yields the gas velocity and liquid velocity in the capillary tube

$$u_g = \frac{1}{4\mu_g}\frac{dp_g}{dx}r^2 + \frac{1}{4\mu_l}\left(\frac{dp_l}{dx} - \rho_l g\right)(r_l^2 - r_b^2) + \frac{r_l^2}{2\mu_l} \times \left(\frac{dp_g}{dx} - \frac{dp_l}{dx} + \rho_l g\right)\ln\left(\frac{r_l}{r_b}\right) - \frac{1}{4\mu_g}\frac{dp_g}{dx}r_l^2, \tag{10}$$

and

$$u_l = \frac{1}{4\mu_l}\left(\frac{dp_l}{dx} - \rho_l g\right)(r^2 - r_b^2) + \frac{r_l^2}{2\mu_l}\left(\frac{dp_g}{dx} - \frac{dp_l}{dx} + \rho_l g\right)\ln\left(\frac{r}{r_b}\right). \tag{11}$$

The liquid pressure gradient, dp_l/dx, in Eqs. (10) and (11) is related to the gas pressure gradient, dp_g/dx, by the Yang–Laplace equation, as:

$$\frac{dp_l}{dx} = \frac{dp_g}{dx} - \frac{dp_c}{dx} = \frac{dp_g}{dx} - \frac{d}{dx}\left(\frac{\sigma_l}{r_l}\right), \tag{12}$$

where σ_l is the liquid surface tension ($N\,m^{-1}$).

The flow rates of gas and liquid in the capillary tube for co-current flow are given as:

$$q_g = 2\pi\int_0^{r_l} u_g r\,dr = \frac{\pi}{4\mu_l}\frac{dp_g}{dx}(r_l^4 - r_l^2 r_b^2) - \frac{\pi r_l^4}{8\mu_g}\frac{dp_g}{dx} - \frac{\pi}{4\mu_l}\left(\frac{dp_c}{dx} + \rho_l g\right)(r_l^4 - r_l^2 r_b^2) + \frac{\pi r_l^4}{2\mu_l}\left(\frac{dp_c}{dx} + \rho_l g\right)\ln\left(\frac{r_l}{r_b}\right), \tag{13}$$

and

$$q_l = 2\pi\int_{r_l}^{r_b} u_l r\,dr = \frac{\pi}{8\mu_l}\left(\frac{dp_c}{dx} + \rho_l g\right)\left[r_b^4 - 4r_b^2 r_l^2 + 3r_l^4 + 4r_l^4\ln\left(\frac{r_b}{r_l}\right)\right] - \frac{\pi}{8\mu_l}\frac{dp_g}{dx}(r_b^2 - r_l^2)^2. \tag{14}$$

By combining Eqs. (12)–(14), the gradient of the radius at the gas–liquid interface, r_l, in the capillary tube may be evaluated as:

$$\frac{dr_l}{dx} = \frac{\pi\rho_l g(AB - CD) - 8\mu_l\mu_g q_g C - 8\mu_l q_l B}{\pi AB - \pi CD}\frac{r_l^2}{\sigma_l}, \tag{15}$$

where

$$A = r_b^4 - 4r_l^2 r_b^2 + 3r_l^4 + 4r_l^4\ln\left(\frac{r_b}{r_l}\right), \tag{16}$$

$$B = 2\mu_g(r_l^4 - r_l^2 r_b^2) - \mu_l r_l^4, \tag{17}$$

$$C = (r_b^2 - r_l^2)^2, \tag{18}$$

and

$$D = 2\mu g\left[r_l^4 - r_l^2 r_b^2 - 2r_l^4\ln\left(\frac{r_l}{r_b}\right)\right]. \tag{19}$$

with corresponding boundary conditions:

$$\text{at } x = 0, \quad r_l = r_{l,0}. \tag{20}$$

where $r_{l,0}$ represents the radius at the gas–liquid interface at the liquid entrance of the capillary tube. Due to the larger ratio of height to radius of the capillary tube and the lower velocity of gas and liquid flow under consideration in this paper, both the liquid flow and the gas flow in the capillary tube can be approximately regarded as fully developed flow, which implies a constant radius profile, and thus the radius at the interface of liquid and gas can be solved from Eq. (15), while letting the left hand side be equal to nil, i.e., $dr_l/dx = 0$, using the Newton iteration method. The liquid film thickness can be obtained for the co-current flow of gas and liquid in the trickling biofilter.

3.2. VOC pollutant transport in the gas core zone, the liquid film zone, and the biofilm zone

Both the biofilm and liquid film are very thin and liquid flow is comparatively slow. It is considered that the VOC only diffuses in the normal direction of the biofilm and the liquid film, i.e., the axial diffusion and convective transport are neglected in these zones. Considering the transport of the VOC in the gas core, the liquid film, and the biofilm with a biological reaction that is evaluated with Andrews-type kinetics, the equations of mass conservation in the three zones may be written as follows.

3.2.1. Mass conservation equation of the VOC and oxygen in the gas core zone

$$u_g \frac{dC_{gT}}{dx} - \left. \frac{2D_{lT}}{r_l} \frac{dC_{lT}}{dr} \right|_{r=r_l} = 0, \tag{21}$$

$$u_g \frac{dC_{gO}}{dx} - \left. \frac{2D_{lO}}{r_l} \frac{dC_{lO}}{dr} \right|_{r=r_l} = 0, \tag{22}$$

with corresponding boundary conditions:

$$\text{at } x = 0, \quad C_{gT} = C_{gT,in} \quad \text{and} \quad C_{gO} = C_{gO,in} \tag{23}$$

where C_{gT} and C_{gO} represent the concentrations of pollutant and oxygen in the gas phase, and C_{lT} and C_{lO} are the concentrations of pollutant and oxygen in the liquid film ($g\,m^{-3}$), respectively. D_{lT} and D_{lO} are the diffusion coefficients of pollutant and oxygen in liquid film ($m^2\,s^{-1}$), respectively. The subscript 'in' represents the parameter at the inlet of the tickling biofilter.

3.2.2. Mass conservation equation of the VOC and oxygen in the liquid film

$$\frac{1}{r}\frac{d}{dr}\left(D_{lT} r \frac{dC_{lT}}{dr}\right) = 0, \tag{24}$$

$$\frac{1}{r}\frac{d}{dr}\left(D_{lO} r \frac{dC_{lO}}{dr}\right) = 0, \tag{25}$$

with corresponding boundary conditions:

$$\text{at } r = r_l, \quad C_{lT} = \frac{C_{gT}}{m_T} \quad \text{and} \quad C_{lO} = \frac{C_{gO}}{m_O} \tag{26}$$

$$\text{at } r = r_l, \quad \frac{dC_{lT}}{dr} = D_{bT}\frac{dC_{bT}}{dr} \text{ and}$$

$$D_{lO}\frac{dC_{lO}}{dr} = D_{bO}\frac{dC_{bO}}{dr} \tag{27}$$

where m_T and m_O are Henry's constants of pollutant and oxygen.

3.2.3. Mass conservation equation of the VOC and oxygen in the biofilm

$$D_{bT}\frac{1}{r}\frac{d}{dr}\left(r\frac{dC_{bT}}{dr}\right) = \frac{X_V}{Y_T}\mu(C_{bT}, C_{bO}, T_b), \tag{28}$$

$$D_{bO}\frac{1}{r}\frac{d}{dr}\left(r\frac{dC_{bO}}{dr}\right) = \frac{X_V}{Y_T}\mu(C_{bT}, C_{bO}, T_b), \tag{29}$$

with corresponding boundary conditions:

$$\text{at } r = r_b + \delta_e, \quad \frac{dC_{bT}}{dr} = 0 \quad \text{and} \quad \frac{dC_{bO}}{dr} = 0 \tag{30}$$

where C_{bT} and C_{bO} stand for the concentrations of pollutant and oxygen in the biofilm ($kg\,m^{-3}$); D_{lT} and D_{lO} are the diffusion coefficients of pollutant and oxygen in the biofilm ($m^2\,s^{-1}$); X_V is the biofilm dry density ($kg\,m^{-3}$); Y_T the yield coefficient of a culture on pollutant ($kg\,kg^{-1}$), and T_b the temperature in the biofilm (°C). $\mu(C_{bt},C_{bo},T_b)$ represents the specific growth rate which depends on the pollutant concentration, the oxygen concentration, and the temperature of the biofilm in the present study. It is shown that the mass transfer behavior has a relation to the temperature profile in a tickling biofilter. The temperature profile needs to be found to predict the treatment efficiency. Furthermore, the exothermic reaction has an impact on the temperature profile. As such, it is necessary to establish a comprehensive heat transfer model coupled with mass transfer and two-phase flow processes of the trickling biofilter in the coming section.

3.3. Heat transfer in the gas core zone, the liquid film zone, and the biofilm zone

The heat conduction in the biofilm is considered to be in the direction normal to the biofilm and the temperature difference along the radial direction in the liquid film and the gas core are neglected. Therefore, the energy conservation equations in the three zones can be written as follows.

3.3.1. Energy conservation equation in the gas core zone and liquid film zone

$$\frac{dT_{gl}}{dx} - \left. \frac{2r_b\lambda_b}{\rho_g c_{p,g} u_g r_l^2 + \rho_l c_{p,l} u_l (r_b^2 - r_l^2)} \frac{dT_b}{dr} \right|_{r=r_b} = 0, \tag{31}$$

with corresponding boundary condition:

$$\text{at } x = 0, \quad T_{gl} = T_{in}, \tag{32}$$

where T_{gl} and T_b represent the temperature in the gas core and liquid film and the temperature in the biofilm (°C), respectively. ρ_g and ρ_l are the gas density and liquid density ($kg\,m^{-3}$). $c_{p,g}$ and $c_{p,l}$ the thermal capacities of the gas and liquid ($J\,kg^{-1}\,K^{-1}$). λ_b is the thermal conductivity of the biofilm ($W\,m^{-1}\,K^{-1}$).

3.3.2. Energy conservation equation in the biofilm

$$\frac{1}{r}\frac{\mathrm{d}}{\mathrm{d}r}\left(\lambda_\mathrm{b} r\frac{\mathrm{d}T_\mathrm{b}}{\mathrm{d}r}\right)+\frac{\Delta H_\mathrm{R}^\mathrm{s} X_\mathrm{V}}{Y_\mathrm{T}}\mu(C_\mathrm{bT}, C_\mathrm{bO}, T_\mathrm{b})=0, \tag{33}$$

with corresponding boundary conditions:

$$\text{at } r=r_\mathrm{b}, \quad T_\mathrm{b}=T_\mathrm{gl}, \tag{34}$$

$$\text{at } r=r_\mathrm{b}+\delta_\mathrm{e}, \quad \frac{\mathrm{d}T_\mathrm{b}}{\mathrm{d}r}=0, \tag{35}$$

where $\Delta H_\mathrm{R}^\mathrm{s}$ is the heat generation ratio of the microorganism metabolizing pollutant ($\mathrm{J\,kg^{-1}}$).

By the end of this section, the two-phase flow, mass transfer, and heat transfer models will have been completely established. The theoretical prediction for treatment efficiency and the thermal behavior of the trickling biofilter operating under different temperature conditions can be obtained if the function for the specific growth rate, pollutant concentration, oxygen concentration, and temperature is employed in the mass transfer equation.

In the next part, experimental data in the present study is used to verify the models. It can be considered that the specific growth rate, μ, has the form of an Andrews-type kinetic dependence as in Eq. (36) due to the fact that the temperature of the packed bed changed within a smaller range in the experiments for a temperature profile.

$$\mu=\mu_\mathrm{max}\frac{C_\mathrm{bT}}{K_\mathrm{T}+C_\mathrm{bT}+(C_\mathrm{bT}^2/K_\mathrm{IT})}\frac{C_\mathrm{bO}}{K_\mathrm{O}+C_\mathrm{bO}}. \tag{36}$$

By combining Eqs. (28), (29), (33) and (36), the corresponding dimensionless Eqs. (21)–(35) are written as follows:

$$\frac{\mathrm{d}C_\mathrm{gT}^*}{\mathrm{d}x^*}-\frac{2h^2}{Pe_\mathrm{T}r_\mathrm{l}^* r_\mathrm{s}^2}\frac{\mathrm{d}C_\mathrm{lT}^*}{\mathrm{d}r^*}\bigg|_{r^*=r_\mathrm{l}^*}=0, \tag{37}$$

$$\frac{\mathrm{d}C_\mathrm{gO}^*}{\mathrm{d}x^*}-\frac{2h^2}{Pe_\mathrm{O}r_\mathrm{l}^* r_\mathrm{s}^2}\frac{\mathrm{d}C_\mathrm{lO}^*}{\mathrm{d}r^*}\bigg|_{r^*=r_\mathrm{l}^*}=0, \tag{38}$$

$$\text{subject to} \quad x^*=0, \quad C_\mathrm{gT}^*=1, \quad C_\mathrm{gO}^*=1, \tag{39}$$

$$\frac{1}{r^*}\frac{\mathrm{d}}{\mathrm{d}r^*}\left(r^*\frac{\mathrm{d}C_\mathrm{lT}^*}{\mathrm{d}r^*}\right)=0, \tag{40}$$

$$\frac{1}{r^*}\frac{\mathrm{d}}{\mathrm{d}r^*}\left(r^*\frac{\mathrm{d}C_\mathrm{lO}^*}{\mathrm{d}r^*}\right)=0, \tag{41}$$

$$\text{subject to} \quad r^*=r_\mathrm{l}^*, \quad C_\mathrm{lT}^*=\frac{C_\mathrm{gT}^*}{m_\mathrm{T}}, \quad C_\mathrm{lO}^*=\frac{C_\mathrm{gO}^*}{m_\mathrm{O}}, \tag{42}$$

$$r^*=r_\mathrm{b}^*, \quad C_\mathrm{lT}^*=C_\mathrm{bT}^*, \quad C_\mathrm{lO}^*=C_\mathrm{bO}^*, \quad \frac{\mathrm{d}C_\mathrm{lT}^*}{\mathrm{d}r^*}=\phi_\mathrm{T}\frac{\mathrm{d}C_\mathrm{bT}^*}{\mathrm{d}r^*}, \quad \frac{\mathrm{d}C_\mathrm{lO}^*}{\mathrm{d}r^*}=\phi_\mathrm{O}\frac{\mathrm{d}C_\mathrm{bO}^*}{\mathrm{d}r^*}, \tag{43}$$

and

$$\frac{1}{r^*}\frac{\mathrm{d}}{\mathrm{d}r^*}\left(r^*\frac{\mathrm{d}C_\mathrm{bT}^*}{\mathrm{d}r^*}\right)=\beta_\mathrm{T}\frac{C_\mathrm{bT}^*}{K_\mathrm{T}^*+C_\mathrm{bT}^*+(C_\mathrm{bT}^{*2}/K_\mathrm{IT}^*)}\frac{C_\mathrm{bO}^*}{K_\mathrm{O}^*+C_\mathrm{bO}^*}, \tag{44}$$

$$\frac{1}{r^*}\frac{\mathrm{d}}{\mathrm{d}r^*}\left(r^*\frac{\mathrm{d}C_\mathrm{bO}^*}{\mathrm{d}r^*}\right)=\beta_\mathrm{O}\frac{C_\mathrm{bT}^*}{K_\mathrm{T}^*+C_\mathrm{bT}^*+(C_\mathrm{bT}^{*2}/K_\mathrm{IT}^*)}\frac{C_\mathrm{bO}^*}{K_\mathrm{O}^*+C_\mathrm{bO}^*}, \tag{45}$$

$$\text{subject to} \quad r^*=\frac{r_\mathrm{b}+\delta_\mathrm{e}}{r_\mathrm{s}}\frac{\mathrm{d}C_\mathrm{bT}^*}{\mathrm{d}r^*}=0, \quad \frac{\mathrm{d}C_\mathrm{bO}^*}{\mathrm{d}r}=0, \tag{46}$$

$$\frac{\mathrm{d}T_\mathrm{gl}^*}{\mathrm{d}x^*}-\beta_\mathrm{gl}\frac{\mathrm{d}T_\mathrm{b}^*}{\mathrm{d}r^*}\bigg|_{r=r_\mathrm{b}^*}=0, \tag{47}$$

$$\text{subject to} \quad x^*=0, \quad T_\mathrm{gl}^*=1. \tag{48}$$

$$\frac{1}{r^*}\frac{\mathrm{d}}{\mathrm{d}r^*}\left(r^*\frac{\mathrm{d}T_\mathrm{b}^*}{\mathrm{d}r^*}\right)+\beta_\mathrm{b}\frac{C_\mathrm{bT}^*}{K_\mathrm{T}^*+C_\mathrm{bT}^*+(C_\mathrm{bT}^{*2}/K_\mathrm{IT}^*)}\frac{C_\mathrm{bO}^*}{K_\mathrm{O}^*+C_\mathrm{bO}^*}=0, \tag{49}$$

$$\text{subject to} \quad r^*=r_\mathrm{b}^*, \quad T_\mathrm{b}^*=T_\mathrm{gl}^*, \tag{50}$$

$$r^*=\frac{r_\mathrm{b}+\delta_\mathrm{e}}{r_\mathrm{s}}, \quad \frac{\mathrm{d}T_\mathrm{b}^*}{\mathrm{d}r^*}=0. \tag{51}$$

where the dimensionless parameters in the above equations are defined as follows:

$$x^*=\frac{x}{h}, r^*=\frac{r}{r_\mathrm{s}}, r_\mathrm{l}^*=\frac{r_\mathrm{l}}{r_\mathrm{s}}, r_\mathrm{b}^*=\frac{r_\mathrm{b}}{r_\mathrm{s}}, C_\mathrm{gT}^*=\frac{C_\mathrm{gT}}{C_\mathrm{gT,in}}, C_\mathrm{gO}^*=\frac{C_\mathrm{gO}}{C_\mathrm{gO,in}}, C_\mathrm{lT}^*=\frac{C_\mathrm{lT}}{C_\mathrm{gT,in}}, C_\mathrm{lO}^*=\frac{C_\mathrm{lO}}{C_\mathrm{gO,in}}, C_\mathrm{bT}^*=\frac{C_\mathrm{bT}}{C_\mathrm{gT,in}}, C_\mathrm{bO}^*=\frac{C_\mathrm{bO}}{C_\mathrm{gO,in}}, K_\mathrm{T}^*=\frac{K_\mathrm{T}}{C_\mathrm{gT,in}}, K_\mathrm{IT}^*=\frac{K_\mathrm{IT}}{C_\mathrm{gT,in}}, K_\mathrm{O}^*=\frac{K_\mathrm{O}}{C_\mathrm{gO,in}}, \phi_\mathrm{T}=\frac{D_\mathrm{bT}}{D_\mathrm{lT}}, \phi_\mathrm{O}=\frac{D_\mathrm{bO}}{D_\mathrm{lO}}, T_\mathrm{gl}^*=\frac{T_\mathrm{gl}}{T_\mathrm{in}}, \text{ and } T_\mathrm{b}^*=\frac{T_\mathrm{b}}{T_\mathrm{in}}.$$

In Eqs. (37) and (38), the Peclet number, $Pe_i=u_\mathrm{g}h/D_{\mathrm{l}i}$, $i=\mathrm{T, O}$, reflects the ratio of the convective mass transport in the gas core zone to the thermal diffusion in the liquid film zone, where h is the height of the packed bed. The dimensionless number β_i, $\beta_i=X_\mathrm{V}\mu_\mathrm{max}r_\mathrm{s}^2/(Y_\mathrm{T}D_{\mathrm{b}i}C_{\mathrm{g}i,\mathrm{in}})$, $i=\mathrm{T,O}$, introduced into Eqs. (44) and (45) represents the ratio of the source intensity of mass to the mass diffusion for the pollutant and the oxygen in the biofilm. The dimensionless number β_gl, $\beta_\mathrm{gl}=2h\lambda_\mathrm{b}r_\mathrm{b}/\{[\rho_\mathrm{g}c_{p,\mathrm{g}}u_\mathrm{g}r_\mathrm{l}^2+\rho_\mathrm{l}c_{p,\mathrm{l}}u_\mathrm{l}(r_\mathrm{b}^2-r_\mathrm{l}^2)]r_\mathrm{s}\}$, in Eq. (47) denotes the ratio of the convective heat transfer in the gas core and the liquid film to the heat conduction in the biofilm and the dimensionless number β_b, $\beta_\mathrm{b}=\Delta H_\mathrm{R}^\mathrm{s}X_\mathrm{V}\mu_\mathrm{max}r_\mathrm{s}^2/\lambda_\mathrm{b}T_\mathrm{in}Y_\mathrm{T}$, in Eq. (49) expresses the ratio of the heat generation rate to the heat conduction in the biofilm.

In addition, the biofilm cannot fully cover the packed material. The surface area of mass transport in the capillary tube is modified through introducing the specific wetted surface area available for biofilm formation. The specific wetted surface area of the biofilm in the trickling biofilter bed, i.e., the area of active

biofilm, could be modified via the following equation [35]:

$$\frac{a_l}{\xi a} = 1 - \exp\left\{-1.45\left(\frac{\sigma_p}{\sigma_l}\right)^{0.75}\left(\frac{Q_l\rho_l}{A_T a\mu_l}\right)^{0.1}\left(\frac{a}{\rho_l^2 g}\right)^{-0.05}\left[\left(\frac{3600Q_l\rho_l}{A_T}\right)^2\frac{1}{\rho_l\sigma_l a}\right]^{0.2}\right\}, \quad (52)$$

where a_l is the active biofilm surface area per unit volume of trickling biofilter (m^{-1}), a the total specific surface area of the packing material (m^{-1}), σ_p the surface tension of the packing material ($N\,m^{-1}$), σ_l the surface tension of liquid ($N\,m^{-1}$), Q_l the liquid flow rate of the trickling biofilter ($m^3\,s^{-1}$), ρ_l the liquid density ($kg\,m^{-3}$), A_T the cross-sectional area of the trickling biofilter column (m^2), μ_l liquid viscosity ($kg\,m^{-1}\,s^{-1}$), and g the gravitational acceleration ($m\,s^{-2}$). The correction factor, ξ, in Eq. (52) is introduced to consider the effect of the liquid–gas flow arrangement and packed sphere size on the wetted biofilm surface area in the trickling biofilter bed in the present model, which was usually adopted by previous research work for the trickling biofilter. For instance, a value of $\xi = 2$ has been reported by Diks and Ottengraf [36,37], a value of ξ was determined in Mpanias and Baltzis's [35] study to be 4.5, and a value of $\xi = 6$ can be inferred from the results of Pedersen and Arvin [38] who speculated that the enlarged contact area between the air and the biofilm may be due to the irregular surface of the biofilm. The correction factor, ξ, for Eq. (52) is a constant determined by fitting the experimental data of the trickling biofilter with the solutions of the theoretical model for a specific gas–liquid flow arrangement and packed sphere size. The active biofilm surface area per unit volume of the trickling biofilter, a_l, is firstly obtained with the present theoretical model using the measured purification efficiency, liquid flow rate, and gas flow rate as the known parameters. The correction factor, ξ, is then calculated with Eq. (52) for various liquid flow rates and gas flow rates under the same packed sphere size and gas–liquid flow arrangement, and finally the mean of all the correction factors is treated as the correction factor of this specific packed material and gas–liquid flow arrangement.

3.4. Numerical solution of the mathematical model

The calculation of the concentration profiles of pollutant and oxygen and the temperature profile in the liquid film zone and biofilm zone proceeds in a stepwise manner as follows:

(1) Discretize the terms with the x-derivatives (d/dx) in Eqs. (37), (38), and (47) using the backward finite difference with an increment Δx, and the terms with r-derivatives (d/dr) in Eqs. (40), (41), (44), (45), and (49) with an increment Δr.
(2) Use the concentrations of pollutant and oxygen at the liquid-biofilm interface and the profiles of pollutant and oxygen concentrations in the biofilm, based on the inlet condition or the previous axial position x for the subsequent increments, to solve the concentration profile of pollutant from Eq. (44) along the r-direction in the biofilm zone and then to solve the concentration profile of oxygen from Eq. (45) using the solution of the pollutant concentration profile.
(3) Obtain new values of concentrations of pollutant and oxygen in the biofilm from solving Eqs. (44) and (45) using the last solution for concentrations of pollutant and oxygen.
(4) Repeat step (3). The iteration process is terminated when two successive values of the pollutant and oxygen concentrations in the biofilm agree within a specific tolerance ($\pm 10^{-3}$).
(5) Solve the concentration profiles of pollutant and oxygen in the liquid film zone from Eqs. (40) and (41) based on the concentration profiles of pollutant and oxygen in the biofilm zone.
(6) Calculate the mass fluxes of pollutant and oxygen at the liquid-biofilm interface from the concentration profiles of pollutant and oxygen in the liquid film zone and from the concentration profiles of pollutant and oxygen in the biofilm zone, respectively.
(7) If the discrepancy between the two values of pollutant or oxygen exceeds $\pm 0.1\%$, the new value of pollutant or oxygen concentration at the liquid-biofilm interface is calculated from the average of the two mass fluxes of pollutant or oxygen at the liquid-biofilm interface.
(8) Repeat steps (2)–(7). The iteration process is halted when two consecutive values of the pollutant or oxygen mass flux at the liquid-biofilm interface agree within a specific tolerance ($\pm 10^{-3}$).
(9) Solve the temperature profile in the biofilm from Eq. (49) using the solutions of the concentration profiles of pollutant and oxygen.
(10) Solve Eqs. (37), (38), and (47) for the pollutant concentration, C^*_{gT}, and the oxygen concentration, C^*_{gO}, in the gas core zone as well as the temperature of gas and liquid, T^*_{gl}, in the gas core zone and the liquid film zone at the next axial position x and then obtain the concentration profiles of pollutant and oxygen and the temperature profile along the axial direction with the same aforementioned steps.
(11) The Tridiagonal Matrix Algorithm (TDMA) method is used in the computation process. Finally, use the temperature rise of the gas and liquid in the gas core and the liquid film to represent the temperature rise of a trickling biofilter along the flow direction of gas and liquid due to the fact that there exists a very slight temperature difference between the gas core zone and the biofilm zone along the radial direction of the capillary tube.

3.5. Parameters for model prediction

The purification performance and the temperature rise of the trickling biofilter for purifying toluene exhaust were calculated. The basic parameters used by the model are shown in Table 1. The relationship of the gas flow rate and the liquid in the capillary tube with the circulation liquid flow rate and the gas flow rate in

Table 1
Parameter values used for solving the model equation

Parameter	Value	Reference
D_{bO} ($m^2\,s^{-1}$)	1.54×10^{-9}	[39]
D_{bT} ($m^2\,s^{-1}$)	0.85×10^{-9}	[39]
D_{lO} ($m^2\,s^{-1}$)	2.41×10^{-9}	[2]
D_{lT} ($m^2\,s^{-1}$)	1.03×10^{-9}	[2]
K_{IT} ($g\,m^{-3}$)	78.94	[2]
K_O ($g\,m^{-3}$)	0.26	[2]
K_T ($g\,m^{-3}$)	11.03	[2]
m_O	34.4	[2]
m_T	0.27	[2]
X_V ($kg\,m^{-3}$)	100.0	[2]
Y_O ($kg\,kg^{-1}$)	0.341	[2]
Y_T ($kg\,kg^{-1}$)	0.708	[2]
δ_e (μm (C_{gT} in $g\,m^{-3}$)	$1.5C_{gT} + 33.4$	[40]
λ_b ($W\,m^{-1}\,K^{-1}$)	0.63	[13]
μ_{max} (h^{-1})	1.5	[2]

the trickling biofilter can be expressed as:

$$q_l = \frac{Q_l}{3600 n_c}, \tag{53}$$

$$q_g = \frac{Q_g}{3600 n_c}, \tag{54}$$

where $n_c = \varepsilon D_T^2 / 4 r_s^2$ is the number of capillary tubes in the packed bed and D_T represents the diameter of the trickling biofilter (m).

It is assumed that carbon dioxide and water are the final products of biodegradation, implying that the carbon combustion heat of toluene equals the sum of the heat generation of the microorganism metabolizing toluene and the combustion heat of the microorganism cells. As a result, the heat generation ratio of the microorganism metabolizing toluene, ΔH_R^s, can be calculated by the following equation [41]:

$$\Delta H_R^s = \Delta H_T - \Delta H_c Y_T, \tag{55}$$

where ΔH_T is the carbon combustion heat of toluene and ΔH_c the combustion heat of the microorganism cells, which is $17.6 \times 10^6\,J\,kg^{-1}$. The carbon combustion heat of toluene is

$$\Delta H_T = \frac{1000 \Delta H_{mT}}{M_T}, \tag{56}$$

where the mole combustion heat of toluene $\Delta H_{mT} = 3.92 \times 10^6\,J\,mol^{-1}$.

The correction factor, ξ, in Eq. (52) was determined by fitting the experimental data with the theoretical solution. In the present study, ξ for the trickling biofilter packed with ceramic spheres 0.018 m in diameter under the gas–liquid co-current flow is 1.0.

3.6. Comparison with experiments

For verifying the model, the theoretical predictions for the temperature rise between the inlet and the outlet of the packed bed were separately compared with the experimental results for toluene removal by the trickling biofilter with ceramic spheres 0.018 m in diameter under gas–liquid co-current flow.

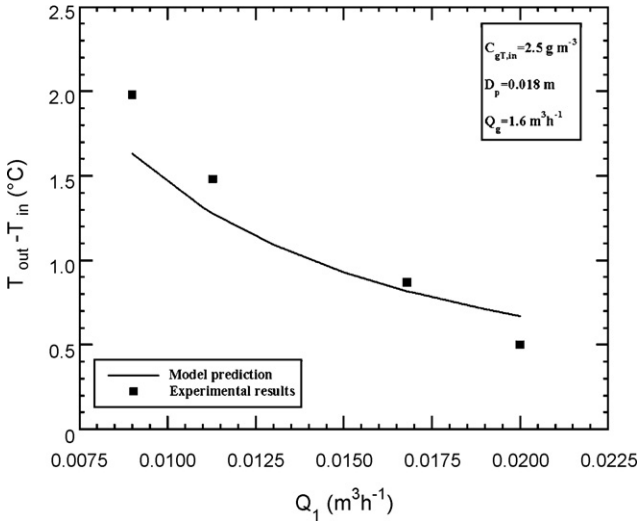

Fig. 11. Variation of the temperature rise between the inlet and outlet of the trickling biofilter versus the liquid flow rate.

The model predictions and experimental results are shown in Figs. 11 and 12, respectively. It can be seen that the model predicted values for the temperature rise are in agreement with the experimental data and the maximum discrepancy between the numerical predictions and the experimental data is less than 29.8%. These figures also show that the predicted temperature rise of the trickling biofilter has a tendency similar to the measured temperature rise, with the temperature rise decreasing with the increase in liquid flow rate and the decrease in gas flow rate at a fixed inlet toluene concentration under gas–liquid co-current flow. It should be noted from Fig. 12 that the model predictions are obviously larger than the experimental data for the inlet toluene concentration of 3.5 g m^{-3}. This is due to the fact that long-term exposure to a higher toluene concentration has a toxic effect on the biofilm and results in the inactivation of a part of the biofilm and a decrease in the treatment efficiency of the trickling biofilter, which is not considered in the present model.

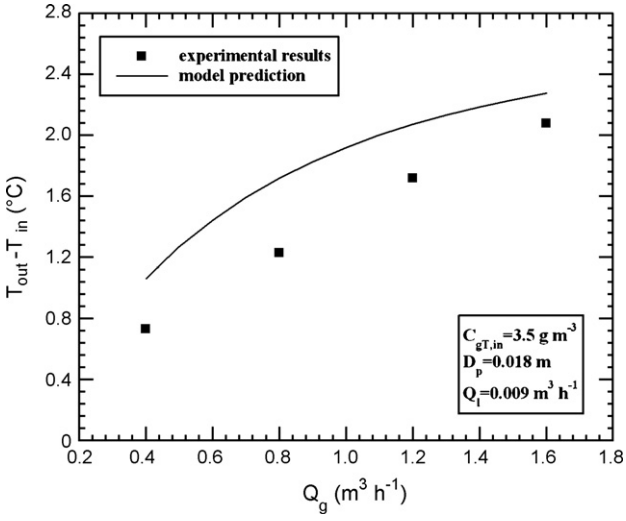

Fig. 12. Variation of the temperature rise between the inlet and outlet of the trickling biofilter versus the gas flow rate.

4. Concluding remarks

Experimental results and theoretical modeling of heat generation characteristics in a trickling biofilter for toluene removal are reported. The experiments show that the temperature of the packed bed had a significant effect on the purification performance of the trickling biofilter and the optimal temperature of the packed bed was between 30 and 40 °C. It was found from the experiments that the temperature of the packed bed gradually rose along the flow direction of gas and liquid under the co-current flow and the temperature rise between the inlet and outlet of the trickling biofilter increased with an increase in the inlet toluene concentration and gas flow rate while it decreased with an increase in the liquid flow rate. The heat generation of the tickling biofilter was modeled by simulating the packed bed as a series of vertical capillary tubes covered by the biofilm. The temperature profile in the trickling biofilter with the gas–liquid co-current flow was calculated by solving the problem of gas–liquid two-phase flow in the capillary tube and the problem of heat and mass transfer through the liquid film and the biofilm in this capillary tube. It is shown that the model, predicting the variations of the temperature rise between the inlet and outlet of the trickling biofilter with increasing gas flow rate and liquid flow rate, is in good agreement with the experimental data.

Acknowledgements

This work was supported by the National Natural Science Foundation of China (Grant no.: 90510020, no.: 50576107), NCET, and SRFDP.

References

[1] S.-J. Hwang, H.-M. Tang, Kinetic behavior of the toluene biofiltration process, J. Air Waste Manage. Assoc. 47 (1997) 664–673.
[2] S.M. Zarook, A.A. Shaikh, Analysis and comparison of biofilter modes, Chem. Eng. J. 65 (1997) 55–61.
[3] H.H. Cox, M.A. Deshusses, Biological waste air treatment in biotrickling filters, Curr. Opin. Biotechnol. 9 (1998) 256–262.
[4] B.C. Baltzis, C.J. Mpanias, S. Bhattacharya, Modeling the removal of VOC mixtures in biotrickling filters, Biotechnol. Bioeng. 72 (4) (2001) 389–401.
[5] H.H.J. Cox, T. Sexton, Z.M. Shareefdeen, M.A. Deshusses, Thermophilic biotrickling filtration of ethanol vapors, Environ. Sci. Technol. 35 (2001) 2612–2619.
[6] X. Zhu, C. Alonso, M.T. Suidan, H. Cao, B.J. Kim, B.R. Kim, The effect of liquid phase on VOC removal in trickle-bed biofilters, Wat. Sci. Tech. 38 (3) (1998) 315–322.
[7] C.J. Mpanias, B.C. Baltzis, Biocatalytic removal of mono-chlorobenzene vapor in trickling filters, Catal. Today 40 (1998) 113–120.
[8] N.Y. Fortin, M.A. Deshusses, Treatment of methyl *tert*-butyl ether vapors in biotrickling filters. 1. reactor startup, steady-state performance, and culture characteristics, Environ. Sci. Technol. 33 (1999) 2980–2986.
[9] M.A. Deshusses, G. Hamer, I.J. Dunn, Behavior of biofilters for waste air biotreatment. 1. Dynamic model development, Environ. Sci. Technol. 29 (1995) 1048–1058.
[10] C.J. Mpanias, B.C. Baltzis, An Experimental and modeling study on the removal of mono-chlorobenzene vapor in biotrickling filters, Biotechnol. Bioeng. 59 (1998) 328–343.
[11] C. Alonso, X. Zhu, M.T. Suidan, B.R. Kim, B.J. Kim, Mathematical model for the biodegradation of VOCs in trickle bed biofilters, Wat. Sci. Tech. 39 (1999) 139–146.
[12] A.H. Wani, R.M.R. Branion, A.K. Lau, Biofiltration: a promising and cost-effective control technology for odors, VOCs and air toxics, J. Environ. Sci. Health 32 (7) (1997) 2027–2055.
[13] A. Rozich, Tackle airborne organic vapors with biofiltration, Environ. Eng. World 1 (1995) 32–34.
[14] G. Wu, B. Conti, G. Viel, A. Leroux, R. Brzezinski, M. Heitz, A high performance biofilter for VOC emission control, J. Air waste Manage. Assoc. 49 (1999) 185–192.
[15] C. Lu, M.-R. Lin, C. Chu, Temperature effects of trickle-bed biofilter for treating BTEX vapors, J. Environ. Eng. 125 (1999) 775–779.
[16] K. Kiared, B. Fundenberger, R. Brzezinski, G. Viel, M. Heitz, Biofiltration of air polluted with toluene under steady state conditions: experimental observations, Ind. Eng. Chem. Res. 36 (11) (1997) 4719–4725.
[17] H. Jorio, L. Bibeau, G. Viel, M. Heitz, Effects of gas flow rate and inlet concentration on xylene vapors biofiltration performance, Chem. Eng. J. 76 (2000) 209–221.
[18] J. Nikiema, L. Bibeau, J. Lavoie, R. Brzezinski, J. Vigneux, M. Heitz, Biofiltration of methane: an experimental study, Chem. Eng. J. 113 (2005) 111–117.
[19] T.O. William, F.C. Miller, Biofilters and facility operations, BioCycle 33 (1992) 75–79.
[20] A. Marsh, Biofiltration for emission abatement, European Coating J. 7–8 (1994) 528–536.
[21] C. Alonso, X. Zhu, M.T. Suidan, B.R. Kim, B.J. Kim, Mathematical model of biofiltration of VOCs: effect of nitrate concentration and backwashing, J. Environ. Eng. 127 (7) (2001) 655–664.
[22] S. Kim, M.A. Deshusses, Development and experimental validation of a conceptual model for biotrickling filtration of H_2S, Environ. Prog. 22 (2) (2003) 119–128.
[23] H. Li, J.R. Mihelcic, J.C. Crittenden, K.A. Anderson, Field measurements and modeling of two-stage biofilter that treats odorous sulfur air emissions, J. Environ. Eng. 129 (8) (2003) 684–692.
[24] Q. Liao, R. Chen, X. Zhu, Theoretical model for removal of volatile organic compound (VOC) air pollutant in trickling biofilter, Sci. China (Ser. E) 46 (3) (2003) 245–258.
[25] Q. Liao, X. Tian, X. Zhu, Y.Z. Wang, R. Chen, H. Liao, Experimental investigation for purification of waste gas containing low concentration toluene in a trickle-bed biofilter, in: Energy and Environment—Proceedings of the International Conference on Energy and Environment, Shanghai, China, December 11–13, Shanghai Scientific and Technical Publishers, 2003, pp. 1643–1648.
[26] C. Alonso, M.T. Suidan, Dynamic mathematical model for the biodegradation of VOCs in a biofilter: biomass accumulation study, Environ. Sci. Technol. 32 (1998) 3118–3123.
[27] R. Mirpuri, W. Jones, J.D. Bryers, Toluene degradation kinetics for planktonic and biofilm-grown cells of *Pseudomones putida* 54 G, Biotechnol. Bioeng. 53 (1997) 535–546.
[28] S. Villaverda, R. Mirpuri, Z. Lewandowski, W.L. Jones, Study of toluene degradation kinetics in a flat plate vapor phase bioreactor using oxygen microsensors, Wat. Sci. Technol. 36 (1997) 77–84.
[29] S. Villaverda, R. Mirpuri, Z. Lewandowski, W.L. Jones, Physiological and chemical gradients in a *Pseudomones putida* 54G biofilm degrading toluene in a flat plate vapor phase bioreactor, Biotechnol. Bioeng. 56 (1997) 361–371.
[30] M. Kaviany, Principles of heat transfer in porous media, second ed., Springer-Verlag publisher, New York, 1995, pp. 32–34.
[31] J. Stark, M. Manga, The motion of long bubbles in a network of tubes, Trans. Porous Media 40 (2000) 201–2181.
[32] C. Hammecker, L. Barbiéro, P. Boivin, J.L. Maeght, E.H.B. Diaw, A Geometrical pore model for estimating the microscopical pore geometry of soil with infiltration measurements, Trans. Porous Media 54 (2004) 193–219.
[33] S.P.P. Ottengraf, A.H.D. van den Oever, Kinetics of organic compound removal from waste gases with a biological filter, Biotechnol. Bioeng. XXV (1983) 3089–3102.
[34] P.A. Jennings, Theoretical model for a submerged biological filter, Biotechnol. Bioeng. 18 (1976) 1249–1273.

[35] C.J. Mpanias, B.C. Baltzis, An experimental and modeling study on the removal of mono-chlorobenzene vapor in biotrickling filters, Biotechnol. Bioeng. 59 (3) (1998) 328–343.
[36] R.M.M. Diks, S.P.P. Ottengraf, Verification studies of a simplified model for removal of dichloromethane from waste gases using a biological trickling filter (Part. I), Bioprocess Eng. 6 (1991) 93–99.
[37] R.M.M. Diks, S.P.P. Ottengraf, Verification studies of a simplified model for removal of dichloromethane from waste gases using a biological trickling filter (Part. II), Bioprocess Eng. 6 (1991) 131–140.
[38] A.R. Pedersen, E. Arvin, Removal of toluene in waste gases using a biological trickling filter, Biodegradation 6 (1995) 109–118.
[39] L. Bibeau, K. Kiared, A. Leroux, et al., Biological purification of exhaust air containing toluene vapor in a filter-bed reactor, Can. J. Chem. Eng. 75 (1997) 921–929.
[40] S. Zarook, B.C. Baltzis, Biofiltration of toluene vapor under steady-state and transient conditions: theory and experimental results, Chem. Eng. Sci. 49 (24) (1994) 4347–4360.
[41] Y.Z. Qi, S.X. Wang, Biochemical reaction kinetics and bioreactor, Chemical Industry Press, Beijing, 1996, pp. 148–149.